Time structure of gamma-ray signals generated in line-of-sight interactions of cosmic rays from distant blazars

Anton Prosekin[1,6], Warren Essey[2], Alexander Kusenko [3,4], and Felix Aharonian[5,1]

ABSTRACT

Blazars are expected to produce both gamma rays and cosmic rays. Therefore, observed high-energy gamma rays from distant blazars may contain a significant contribution from secondary gamma rays produced along the line of sight by the interactions of cosmic-ray protons with background photons. Unlike the standard models of blazars that consider only the primary photons emitted at the source, models which include the cosmic-ray contribution predict that even ~ 10 TeV photons should be detectable from distant objects with redshifts as high as $z \geq 0.1$. Secondary photons contribute to signals of point sources only if the intergalactic magnetic fields are very small, $B \lesssim 10^{-14}$ G, and their detection can be used to set upper bounds on magnetic fields along the line of sight. Secondary gamma rays have distinct spectral and temporal features. We explore the temporal properties of such signals using a semi-analytical formalism and detailed numerical simulations, which account for all the relevant processes, including magnetic deflections. In particular, we elucidate the interplay of time delays coming from the proton deflections and from the electromagnetic cascade, and we find that, at multi-TeV energies, secondary gamma-rays can show variability on timescales of years for $B \sim 10^{-15}$ G.

Subject headings: gamma rays, cosmic rays, active galaxies

[1]Max Planck Institute, Heidelberg, Germany

[2]ICCS, University of California, Berkeley, CA 94708-1003, USA

[3]Department of Physics and Astronomy, University of California, Los Angeles, CA 90095-1547, USA

[4]Kavli Institute for the Physics and Mathematics of the Universe, University of Tokyo, Kashiwa, Chiba 277-8568, Japan

[5]School of Cosmic Physics, Dublin Institute for Advanced Studies, 31 Fitzwilliam Place, Dublin 2, Ireland

[6]Fellow of the International Max Planck Research School for Astronomy and Cosmic Physics at the University of Heidelberg (IMPRS-HD)

1. Introduction

Active Galactic Nuclei (AGN) are expected to be sources of both cosmic rays and gamma rays. While gamma rays have been observed from a number of blazars, the identification of cosmic rays with their sources is impossible (except at the highest energies), because the Galactic magnetic fields change their directions considerably. However, as long as the intergalactic magnetic fields are relatively small, cosmic rays produced in blazars can travel close to the line of sight and produce secondary gamma rays which would significantly contribute to the radiation observed from the direction of the point sources. For nearby blazars such contributions are expected to be small in comparison with direct gamma-ray signals reaching Earth. However, for more distant blazars, the line-of-sight produced gamma rays can dominate over the direct gamma rays from the source (Essey & Kusenko 2010). The transition occurs because the primary gamma rays are filtered out in their interactions with extragalactic background light (EBL), while the fraction of secondary gamma rays produced by cosmic rays in intergalactic space grows with distance traveled. Based on the spectra of individual blazars (Essey & Kusenko 2010; Essey et al. 2010, 2011a) and on the trend in spectral softening (Essey & Kusenko 2011), one expects the secondary contribution to be important for redshifts $z > 0.15$ and energies $E > 1$ TeV.

The intrinsic gamma-ray spectra of some blazars, after correction for absorption in EBL, appear extremely hard, challenging the standard, e.g. the synchrotron-self-Compton (SSC) or External Compton models of blazars. Several solutions to this problem have been proposed. Intergalactic cascading of gamma rays from blazars in the case of very weak intergalactic magnetic fields (IGMFs) can increase the effective mean free path of gamma-rays (Aharonian et al. 2002; Taylor et al. 2011), however, for distant blazars this effect alone appears to be insufficient to explain the gamma-ray spectra above 1 TeV. The very hard spectra of primary gamma rays (Katarzyński et al. 2006; Stecker & Scully 2007; Lefa et al. 2011), or special features in the sources (Aharonian et al. 2008) can help reconcile the data with theoretical predictions, at the cost of introducing some *ad hoc* assumptions. Hypothetical new particles (de Angelis et al. 2007; Horns & Meyer 2012) and Lorentz invariance violation (Protheroe & Meyer 2000) have been invoked to explain the data.

The inclusion of cosmic-ray contribution offers an alternative solution to the problem. Indeed, since a significant fraction of gamma rays in this model is produced relatively close to the observer, this model reduces dramatically the impact of gamma-ray absorption in EBL. This is illustrated in Fig. 1. Protons with energy $E \geq 10^{16}$ eV propagating through weak IGMFs without strong deviations from the line of sight can carry energy from the source close to the observer and can generate a substantial gamma-ray flux at multi-TeV energies. Remarkably, the predicted spectra of secondary gamma rays depend only on the

source redshift (determined from independent observations). For each source, the power emitted in cosmic rays is the only fitting parameter which can be used to fit the data. As long as the source redshifts are known, the predictions of this model are solid and robust. The spectra calculated for the redshifts of all observed distant blazars provide a very good fit to observational data (Essey & Kusenko 2010; Essey et al. 2010, 2011a; Murase et al. 2011), with a reasonable required luminosities in cosmic rays assuming that the escape of protons from the source is strongly beamed toward the observer (Essey et al. 2011a; Razzaque et al. 2012).

Confirmation of this model by future observations will have several important consequences. It will imply that (i) cosmic rays are, indeed, accelerated in AGN, as has long been suspected, but never before confirmed by observations; (ii) intergalactic magnetic fields are fairly small, of the order of several femtogauss (10^{-15} G) or lower (Essey et al. 2011b); and (iii) the problem of intergalactic gamma-rays can be somewhat relaxed, and consequently the upper limits on EBL derived while neglecting the cosmic-ray contributions may need be revised. Within this model, the expected temporal structure of signals from distant blazars at the highest energies should reflect the time delays cosmic rays undergo in the intergalactic magnetic fields. We note that while time variability has been observed for *nearby* TeV blazars at TeV energies and for distant TeV blazars at energies above a few hundred GeV, no variability has been reported so far for *distant* TeV blazars at *TeV energies*. Here we call *distant* those blazars that have large enough redshifts for the primary TeV gamma-rays to die out. Based on the spectral fits (Essey & Kusenko 2010; Essey et al. 2010, 2011a; Murase et al. 2011), and the spectral softening of blazars Essey & Kusenko (2011), one concludes that most blazars with redshift $z \geq 0.15$ should fall in this category. Since the ratio of gamma-ray luminosity to cosmic-ray luminosity can vary from source to source, one expects a mixed population to exist at some intermediate redshifts $0.1 < z < 0.15$, where stronger cosmic ray emitters should be observed in secondary gamma rays, while stronger gamma ray emitters should be observed in primary gamma rays. Furthermore, if stronger IGMFs exist in the directions of specific sources, the secondary contribution can be suppressed. For example, PKS 2155-304 at $z = 0.12$ is an example of a source at an intermediate redshift from which primary signals are observed, as indicated by its TeV variability HESS Collaboration (2010). Whether the lack of TeV variability is a generic feature of distant blazars, or merely an artifact of low statistics in multi-TeV photons, should be clarified in future observations. An important issue in this context is the knowledge of the spectral and temporal features of the radiation predicted by the model. The spectral features of the radiation have been studied in detail by Essey et al. (2011a).

In this paper we consider the extent to which the time variability at high energies should be erased by the cosmic ray propagation delays. We will focus on calculating the Green's

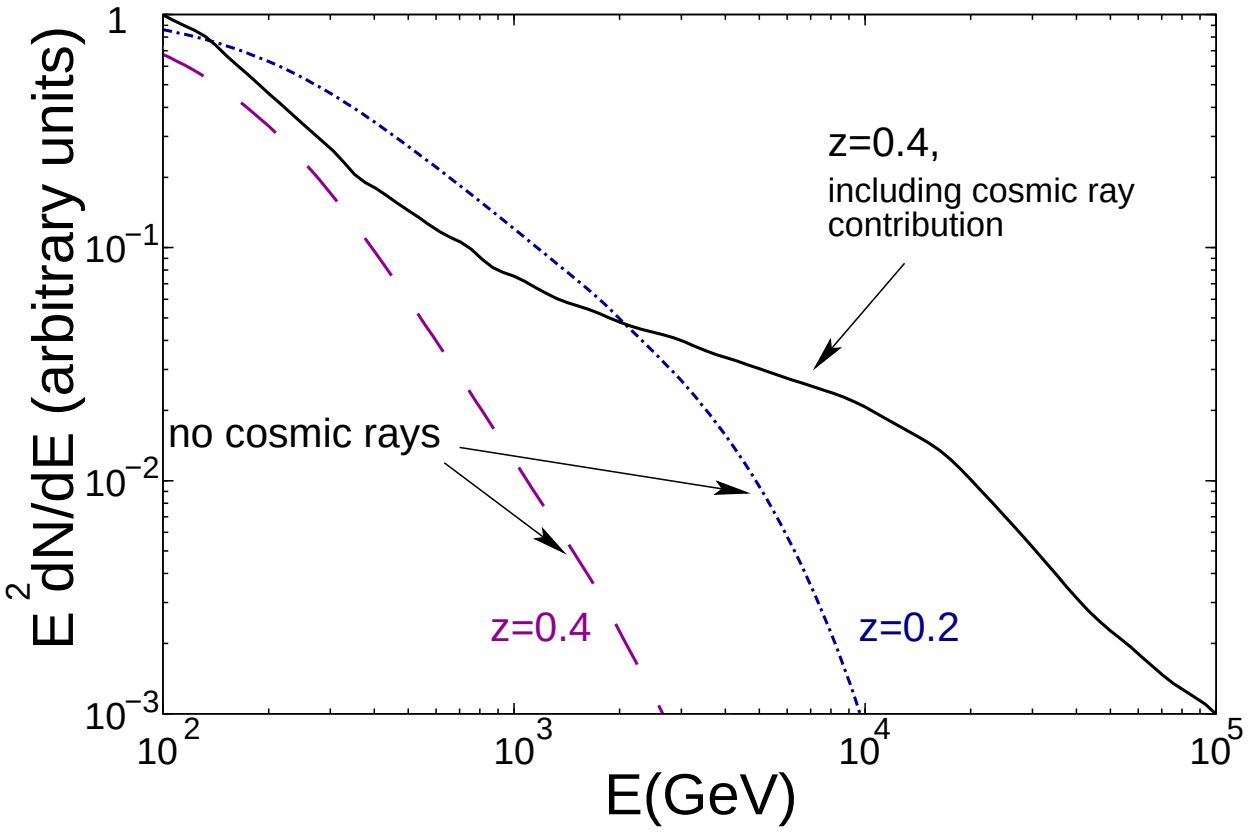

Fig. 1.— Secondary gamma rays produced in line-of-sight interactions of cosmic rays result in harder spectra for distant sources. Since most of the observed photons are produced relatively close to the observer, there is less attenuation due to the interactions with EBL.

function, which corresponds to a time delay from an infinitely narrow pulse of protons at the source. Realistic time profiles can be obtained by convolving the time-dependent source luminosity with this Green's fucntion. However, since a fair fraction of the blazar flaring activity occurs on the time scales much sorter than those we discuss below, in many cases the Green's function can be interpreted as a distribution of photon arrival times from a flaring source. In applications of our method to data analysis, one can employ time-dependent templates inferred from lower energies.

2. Basic estimates and scaling laws

There is no doubt that, for nearby blazars, the primary gamma rays produced at the source are responsible for most of the observed radiation. While these objects can also produce cosmic rays, the contribution of secondary gamma rays is not expected to dominate. However, for larger distances, the primary gamma-ray component is filtered out above a TeV, while the secondary contribution is enhanced. Indeed, the scaling of the primary gamma rays with distance is determined by the losses due to pair production in gamma-ray interactions with extragalactic background light (EBL):

$$F_{\mathrm{primary},\gamma}(d) \propto \frac{1}{d^2}\exp(-d/\lambda_\gamma). \tag{1}$$

In contrast, gamma rays generated in line-of-sight interactions of cosmic rays exhibit a very different scaling with distance (Essey & Kusenko 2010; Essey et al. 2010, 2011a):

$$\begin{aligned} F_{\mathrm{secondary},\gamma}(d) &\propto \frac{\lambda_\gamma}{d^2}\left(1-e^{-d/\lambda_\gamma}\right) \\ &\sim \begin{cases} 1/d, & \text{for } d \ll \lambda_\gamma, \\ 1/d^2, & \text{for } d \gg \lambda_\gamma. \end{cases} \end{aligned} \tag{2}$$

Here λ_γ is the distance at which EBL opacity to TeV gamma rays is of the order of 1. The lack of suppression is due to the fact that the photon backgrounds (CMB and EBL) act as a target on which gamma rays are produced by the cosmic rays. Hence, a higher column density of background photons for a more distant source boosts, not hinders the gamma-ray production.

As long as IGMFs are weak enough to cause only small deflections, for a sufficiently distant source, secondary gamma rays dominate because they don't suffer from exponential suppression as in Eq. (1), which is absent from Eq. (2). The transition from primary to secondary photons occurs when the optical depth to pair production exceeds 1. The corresponding redshift can also be inferred from the spectral softening of the spectra (Essey & Kusenko

2011). Based on these estimates, one can expect the secondary gamma rays to dominate for sources at redshifts $z \gtrsim 0.15$.

The success of the spectral fits to the data for secondary gamma rays (Essey & Kusenko 2010; Essey et al. 2010, 2011a) can be interpreted as possible evidence of cosmic ray acceleration in blazars. Within this interpretation, the beamed energy output in $E > 10^{17}$ eV cosmic rays required to fit the observed spectra of distant blazars is of the order of 10^{43} erg, or 10^{45} erg isotropic equivalent (Essey & Kusenko 2010; Essey et al. 2010, 2011a), which is consistent with many models (Berezinsky et al. 2006). The luminosity required to explain ultrahigh-energy cosmic rays (UHECR) depends on the assumed spectrum, which is often parameterized by a broken power law with a break at some value E_c (unknown a priori). According to Berezinsky et al. (2006), the AGN luminosities in cosmic-ray protons needed to account for the UHECR data are 5.6×10^{43} erg/s, 2.5×10^{44} erg/s, and 1.1×10^{45} erg/s, for $E_c = 10^{18}$ eV, $E_c = 10^{17}$ eV, and $E_c = 10^{16}$ eV, respectively. These estimates are in general agreement with our results. We also note that, because of the selection effects, the sources observed from large distances are by no means average: they are the brightest AGNs, which generate exceptional power in cosmic rays.

The spectra of observed gamma rays generated in this fashion depend on the intervening intergalactic magnetic fields. It is easy to understand some qualitative features of this dependence in terms of a simplified random-walk description of the proton propagation. Let us consider a short pulse of protons emitted from a source at distance d. At later times, the proton pulse broadens and takes the shape $f(t, r)$. The explicit form of $f(t, r)$ was computed by Aharonian et al. (2010) and will be discussed below. (See also Alcock & Hatchett (1978); Williamson (1972).)

At every point in its trajectory, the proton interactions with the cosmic background generate a flux of gamma rays, which quickly (on a kpc length scale) cascade down to energies below the threshold. From that point on, gamma rays travel without further time delays. However, during the cascade development, the IGMFs cause some delays (which are longer than the delays of the protons in the IGMFs for E_γ below 10 TeV).

Let us consider the proton propagation in IGMFs. We assume that IGMFs form a lattice with correlation length l_c, in which a proton with energy $E_p = 10^{17}$eV random-walks over a distance $d \sim 1000\,\mathrm{Mpc} = n \times l_c$, where $n \sim 10^3$.

The angle between the proton momentum and the line of sight performs a two-dimensional random walk in small steps of $\sim 10^{-6}$. When the proton interacts with a background photon, it emits a narrow shower in the direction of the proton's momentum. The prompt gamma rays are emitted into a narrow angle $(\sim E_p/\mathrm{MeV})^{-1}$ for Bethe–Heitler pair production, or

($\sim E_p/0.2\,\mathrm{GeV})^{-1}$ for pion photoproduction. The cascade develops and broadens this angle, with larger angles at lower energies. To shower in the direction of observer after n steps of random walk, the proton angle should return to 0. For a 2D random walk, the probability of *not* returning to zero after n steps is $\gamma_2(n) = \frac{\pi}{\ln n} + O\left(\frac{1}{(\ln n)^2}\right)$. This probability drops below 1/2 for $n > \exp(2\pi) \sim 5 \times 10^2$. For $d \sim 1000\,\mathrm{Mpc}$, $n \sim 10^3$, and so each proton angle returns to the origin about ~ 1 time per distance traveled. Therefore, the diffusion approximation is justified, and a "typical" delay can be computed using the distance traveled, assuming the random walk.

Deflection of a proton in a single cell is θ_0. This deflection and the time delay are determined by the Larmor radius

$$R_B = \frac{E}{eB} = 10^5 \mathrm{Mpc}\ E_{p,17}/B_{-15},$$

where $E_{p,17}$ is the proton energy in units of 10^{17} eV, and B_{-15} is the value of the magnetic field in femtogauss.

Therefore,

$$\theta_0 = \frac{l_c}{R_B} = 10^{-5} \left(\frac{l_c}{\mathrm{Mpc}}\right)\ B_{-15}/E_{p,17}.$$

Time delay in crossing a single cell is

$$\Delta t_0 = \frac{l_c}{c}\theta_0^2 = 10^4 \mathrm{s} \left(\frac{B_{-15}}{E_{p,17}}\right)^2.$$

After $n \sim 10^3$ steps of random walk, the time delay is

$$\tau_p = n\Delta t_0\ \sim 10^7 \mathrm{s} \left(\frac{B_{-15}}{E_{p,17}}\right)^2. \tag{3}$$

Significant time delays are also incurred in the EM showering process. Each observed gamma ray was at some point an electron in the cascade. The time delay of each gamma ray with an observed energy E_γ is dominated by the delay during the lowest-energy "electron" phase of this gamma ray. The electron energy is related to the energy of observed IC γ ray by $E_\gamma \propto E_e^2$. IGMFs act on the electron over a distance of the order of its cooling distance $D_e \propto 1/E_e$. The time delay incurred in this process is proportionate to the sum (Ichiki et al. 2008; Murase et al. 2008) of D_e and the mean free path to pair production λ_{PP}, which has the same energy dependence (with a much larger prefactor), $\lambda_{\mathrm{PP}} \propto 1/E_e$. The resulting delay is

$$\tau_e = (\lambda_{\mathrm{PP}} + D_e)\theta_e^2/c, \text{ where } \theta = D_e \frac{eB}{E_e}.$$

Therefore,

$$\tau_\gamma \approx \tau_e = D_e^2(\lambda_{\rm PP} + D_e)\frac{e^2B^2}{cE_e^2} \propto \frac{B^2}{E_e^5} \propto \frac{B^2}{E_\gamma^{5/2}} \tag{4}$$

where we have assumed $D_e \sim$ kpc $\ll l_c$.

The proton delay (3) is

$$\tau_p \propto \frac{B^2}{E_p^2}. \tag{5}$$

The total time delay of an observed photon is the sum of τ_p and τ_γ:

$$\tau_{\rm tot} = \tau_p + \tau_\gamma = C_1\frac{B^2}{E_p^2} + C_2\frac{B^2}{E_\gamma^{5/2}}, \tag{6}$$

where C_1 and C_2 are some constants.

One can, therefore, expect the following structure of time delays. The shortest delay time is determined by the delay in the arrival of the highest-energy proton; this time delay is given by Eq. (5). High-energy protons travel faster than the gamma-ray cascades, and they are followed by a tail of trailing gamma rays. There are two contributions to the total delay time, which have a different dependence on energy (6). As the second term in Eq. (6) diminishes with energy, the time delay approaches a plateau independent of the photon energy. The height of this plateau is determined by the energy of the proton. This agrees with the results of numerical caclculations presented in Figure 2.

3. Semi-analytical description

Let us consider the time delays due to the propagation of protons. Protons interactions with extragalactic background radiation (both CMB and EBL) occur with a very low probability for energies below the pion production threshold. In the pair production process, a proton loses only $\sim 10^{-3}$ of its energy in each collision. Thus, one can neglect the energy losses for protons in making some basic estimates. (However, in our numerical calculations, we take into account all the energy losses, including adiabatic losses.) Also, the deflection angles can be assumed small for the relevant range of parameters. Calculation of the electromagnetic cascade initiated by the secondary gamma rays produced in proton-photon interactions is much more difficult, and there is no simple analytical approach that could allow one to calculate the distribution function of gamma rays. Therefore we will employ a hybrid approach by combining an analytical treatment of protons with a Monte Carlo simulation for the electromagnetic cascade.

To calculate the distribution function of protons, let us consider a mono-energetic beam of protons emitted with energy E at some point in time. Random deflections in weak IGMFs result in arrival time distribution which is convenient to consider as a function of time delay parameter $\tau = t - r/c$, where r is the distance to the source and c is the speed of light. In a small-angle approximation, one can express the distribution function as follows (Aharonian et al. 2010):

$$f_A(E,\tau,r) = \frac{1}{\tau}\left(\frac{c\tau}{r^2\langle\theta_s^2\rangle}\tilde{f}_A\left(\frac{c\tau}{r^2\langle\theta_s^2\rangle}\right)\right), \tag{7}$$

where

$$\tilde{f}_A(y) = 4\pi^2\sum_{n=1}^{\infty}(-1)^{n-1}n^2e^{-2\pi^2n^2y} \tag{8}$$

$$\langle\theta_s^2\rangle = \frac{l_c}{5}\left(\frac{e}{E}\right)^2\langle B^2\rangle. \tag{9}$$

Here $\langle\theta_s^2\rangle$ is the mean square deflection angle per unit length. The correlation length l_c and the mean square of magnetic field $\langle B^2\rangle$ enter in Eq. (7) as parameters. The normalization of the function f_A is so that $\int_0^\infty f_A d\tau = 1$. Then the distribution function of protons injected with energy spectrum $J_p(E)$ at the distance r from the source is

$$f_p(E,\tau,r) = \frac{J_p(E)f_A(E,\tau,r)}{r^2}. \tag{10}$$

Let protons interact with low energy photon field $f_{ph}(\epsilon)$. The protons with a monoenergetic distribution (normalized to one particle) produce electron-positron pairs at the rate $\Phi(E_e, E_p)$, where E_p is the energy of protons, E_e is the energy of pairs. Following Kelner & Aharonian (2008), one can express $\Phi(E_e, E_p)$ as follows:

$$\Phi(E_e,E_p) = c^2\int d\epsilon\frac{d\Omega}{4\pi}f_{ph}(\epsilon)\frac{k\cdot u_p}{\epsilon\gamma_p}\int\delta(E_e - c(u_{lf}\cdot p_e))d\sigma\,, \tag{11}$$

where k, u_p, and u_{lf} are four-velocities of photon, proton, and the laboratory frame, respectively; and p_e is four-momentum of electron (or positron). γ_e and ϵ are the proton Lorentz factor and the energy of photon in the laboratory frame. $d\sigma$ is the Bethe-Heitler cross section. The photon field used in this calculations includes the CMB and EBL, and one can neglect the redshift evolution.

Then distribution function of electrons produced at the distance r with inherited time delay τ is

$$f_e(E_e,\tau,r) = \int dE_p\frac{J_p(E_p)f_A(E_p,\tau,r)}{r^2}\Phi(E_e,E_p). \tag{12}$$

These electrons initiate an electromagnetic cascade. Let $f_{cas}(E_e, E_\gamma, s)$ be the number of photons with energy E_γ produced in the cascade initiated by an electron with energy E_e at the distance s from the observer and detected at the point of observation. The mean time delay of the photons is $\tau_{cas}(E_e, E_\gamma, s)$. The extragalactic magnetic field is a parameter. Then for the UHE proton source at the distance d the number of photons produced in the cascade with time delay $\tau = \tau_{cas} + \tau_{prot}$ is

$$f_\gamma(E_\gamma, \tau, d) = \int_0^d dr \int dE_e f_e(E_e, \tau - \tau_{cas}(E_e, E_\gamma, r), d - r) f_{cas}(E_e, E_\gamma, r) \qquad (13)$$

The Eqs. (7), (12) and (13) constitute the integral which is calculated numerically. The functions f_{cas} and τ_{cas} actually depend on redshift but not on distance, therefore we use the relation

$$dr = \frac{c}{H_0} \frac{1}{(1+z)\sqrt{(1+z)^3\Omega_m + \Omega_\Lambda}} dz, \qquad (14)$$

to express distance via redshift and perform integration over z.

We assume that the source produces a power-law spectrum of protons with a spectral index α and the energy range from $0.1E_0$ to E_0. The results for the mean time delay of gamma rays are presented in Figs. 2 and 3 as a function of the varying cut-off energy, distance to the source and spectral index. In these calculations we assumed that the intergalactic magnetic field has the strength $B = 10^{-15}$ G and the coherence length $l_c = 1$ Mpc. Unless specified otherwise, we use $E_0 = 10^{17}$ eV, $\alpha = 2$.

The advantage of the analytical description presented above is the possibility to study the time delay distribution of gamma rays for a variety of initial proton spectrum parameters. The numerical Monte Carlo approach described below has computational limitations on the number of initial particles, which can complicate the study of how a proton spectrum with a wide energy range can affect the time delays of gamma rays. The protons injected with slightly different energies would have the time distribution which is similar to the time distribution for a monoenergetic proton beam. In contrast, the time distribution of protons with a broad energy spectrum is a sum of time distributions of protons with different energies, which is stretched out in time. This would spread the arrival times of gamma rays along a large time span. The illustration of this effect can be seen from the comparison of the second panel of Fig. 4 and Fig. 5. The range of the proton energies has a strong effect on the lower energy gamma rays, whereas the time distribution for $E_\gamma = 1 \cdot 10^{14}$ eV does not change significantly. This is because, in the case of a broad spectrum, protons with different energies can contribute gamma rays of a given energy. On the other hand, only the protons of highest energies are responsible for the production of gamma rays of $E_\gamma = 1 \cdot 10^{14}$ eV.

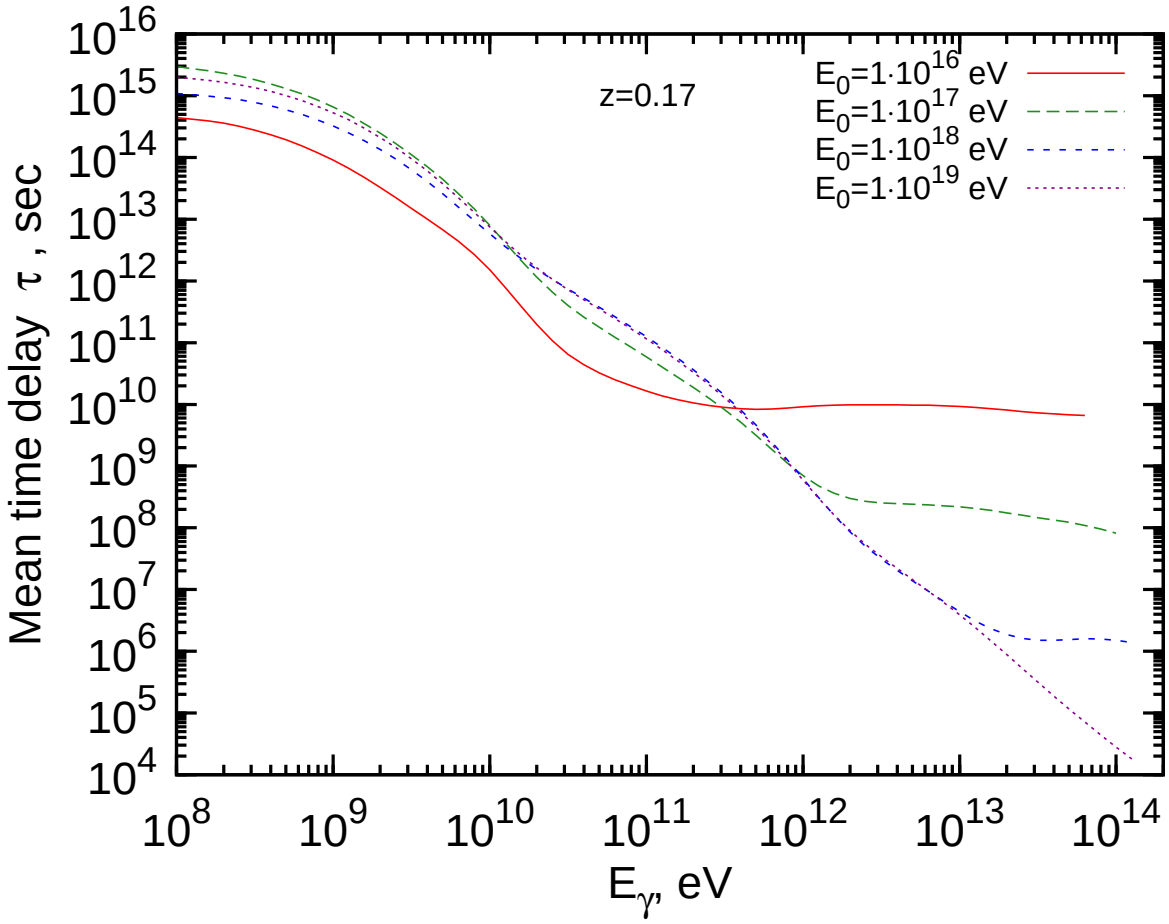

Fig. 2.— Mean time delay of gamma rays at redshift $z = 0.17$ for different cutoff energies E_0 of proton spectrum.

Therefore, the corresponding time distribution is similar to the one for the monoenergetic protons (*cf.* Fig. 6).

The flux of gamma rays arriving at any given time comprises contributions from protons at different points along the line of sight. We obtain this flux by integrating over the proton distributions shifted by a time delay incurred in the electromagnetic cascade. The latter delays were obtained from numerical calculations using a single Monte Carlo numerical run. The results are shown in Figs. 4 and Fig. 5. The multiple-peak structure apparent in these curves is the result of adding contributions from different distances with the delay profile obtained from a single numerical run. If we adopted a different approach and used an averaged delay profile, as in Fig. 7, the "many-peak" structure would be erased.

4. Numerical Monte-Carlo calculations

In addition to the semi-analytical results we also performed a full scale Monte Carlo simulation to track the arrival times of individual particles. The source was modeled by an instantaneous pulse of protons to represent the Green's function needed to calculate the distribution of arrival times. Particles are advanced in time steps of roughly $0.1 - 1$ kpc, updating momentum, position and time delay with all relevant interactions taken into account. Gamma rays arriving at the $z = 0$ surface are binned and the mean arrival time and standard deviation are calculated.

The proton energy loss processes are well studied (Szabo & Protheroe 1994) and can be described by a standard approach. We calculate all the relevant energy losses, including adiabatic losses and the losses due to the interactions with photon backgrounds. The most important contributions to secondary photon production are photopion production and proton pair production (PPP).

The photopion production processes involve the following reactions:

$$\begin{aligned} p + \gamma_b &\rightarrow n + \pi^+ \\ p + \gamma_b &\rightarrow p + \pi^0 \end{aligned} \tag{15}$$

where γ_b is either a CMB or EBL photon. PPP occurs in the reaction

$$p + \gamma_b \rightarrow p + e^+ + e^-. \tag{16}$$

The pair production on the CMB is the dominant reaction, but pion photoproduction on EBL also contributes. Pion photoproduction on CMB has a threshold above 10^{19} eV, but pion production on EBL is possible for all energies we consider. The efficiency of energy

transfer to the electromagnetic shower depends on the proton energy and on the distance to the source. A more detailed discussion is presented elsewhere (Aharonian et al. 2012).

The mean interaction length, λ, for a proton of energy E traveling through a photon field is given by

$$[\lambda[E]]^{-1} = \frac{1}{8\beta E^2} \int_{\epsilon_{\min}}^{\infty} \frac{n(\epsilon)}{\epsilon^2} \int_{s_{\min}}^{s_{\max}(\epsilon,E)} \sigma(s)(s - m_p^2) ds d\epsilon, \tag{17}$$

where $n(\epsilon)$ is the differential photon number density of photons of energy ϵ, and $\sigma(s)$ is the appropriate total cross section for the given process for the center of momentum (CM) frame energy squared, s, given by

$$s = m_p^2 + 2\epsilon E(1 - \beta \cos\theta), \tag{18}$$

where θ is the angle between the proton and photon, and β is the proton's velocity.
For pion photoproduction,

$$s_{\min} = (m_p^2 + m_\pi^2)^2 \tag{19}$$

and

$$\epsilon_{\min} = \frac{m_\pi(m_\pi + 2m_p)}{2E(1+\beta)}. \tag{20}$$

For proton pair production

$$s_{\min} = (m_p^2 + 2m_e^2)^2 \tag{21}$$

and

$$\epsilon_{\min} \approx \frac{m_e(m_e + m_p)}{E}. \tag{22}$$

For both processes,

$$s_{\max}(\epsilon, E) = m_p^2 + 2\epsilon E(1+\beta). \tag{23}$$

Both pions and neutrons quickly decay via the processes

$$\begin{aligned} n &\rightarrow p + e^- + \bar{\nu}_e, \\ \pi^+ &\rightarrow \mu^+ + \nu_\mu \rightarrow e^+ + \nu_e + \bar{\nu}_\mu + \nu_\mu, \\ \pi^0 &\rightarrow 2\gamma. \end{aligned} \tag{24}$$

The outgoing distribution functions for pion photoproduction were generated using the SOPHIA package Mücke et al. (2000).

Primary gamma rays and gamma rays produced from the above equations can interact and pair-produce on background photons. The resulting electron positron pairs will IC scatter CMB photons. The upscattered photons can once again pair produce, this chain

reaction is known as electromagnetic (EM) showering.
The interaction length for photons for pair production off the EBL is

$$[\lambda]^{-1} = \Big(\frac{m_e^2}{E}\Big)^2 \int_{\frac{m_e^2}{E}}^{\infty} \epsilon^{-2} n(\epsilon) \int_1^{\frac{\epsilon E}{m_e^2}} 2s\sigma(s) ds d\epsilon, \tag{25}$$

where

$$\sigma = \frac{1}{2}\pi\Big(\frac{e^2}{m_e^2}\Big)^2 (1-\beta^2)\Big[(3-\beta^4)\ln\frac{1+\beta}{1-\beta} - 2\beta(2-\beta^2)\Big] \tag{26}$$

and

$$\beta = (1-1/s)^{1/2}, \tag{27}$$

and $n(\epsilon)$ is the differential photon number density of photons of energy ϵ.

To simulate magnetic field effects, the IGMF is modeled by cubic cells of a given magnetic field strength with sides equal to the chosen correlation length, l_c, and a random direction. Particles are moved forward in fine time steps and the deflection of the particle is calculated using the Larmor radius and IGMF direction. Time delays for charged particles are calculated in comparison to a photon traveling in a straight line to the observer.

For the analysis of time delays, we have performed multiple runs and averaged the results, as shown in Fig. 7.

The results of the simulation are shown in Fig. 8, where delays from deflections in the IGMF are shown for a source at $z = 0.2$. It is evident that secondary photons produced at large distances conform to the power-law behavior as in Eq. (4). This approximate power law is illustrated in Fig. 8 by a dashed line. The flattening at low energies can be understood by the way the code handles deflections. Particles are moved forward in time steps of roughly $0.1 - 1$ kpc and deflections are assumed to be less than π within a single time step. For the lowest energies this is not always true and the code will underestimate the deflection, thus producing time delays below the power law.

5. Discussion and conclusion

The main qualitative features of the Green's function computed numerically and shown in Fig. 2 and Fig. 8 can be easily understood. For lower energies (below TeV), time delays $\tau \propto B^2 E^{-5/2} d$, where d is distance to the source. The nearby showers arrive before distant showers, so that the late arriving gamma rays have lower energies and longer delays. The plateau that develops at $E > 1$TeV is due to the prompt showers emitted by the protons nearby, for which the time delays are determined by the proton deflections in IGMFs. In the

absence of cosmic rays, the spectrum would drop above 1 TeV, and the multi-TeV gamma rays would not be observed.

For sub-TeV secondary gamma rays the electromagnetic cascade delays are always longer than the proton delays, and the arrival photons peak at the time given by Eq. (4). At energies above TeV, the proton delays come to dominate, in accordance with the broken power law in Eq. (6). The numerical results differ somewhat from the scaling in Eq. (6). In particular, at low energies, the delays appear to scale as E^{-2} rather than $E^{-2.5}$. The difference can be explained by a combination of several effects. For electron energies below 30 GeV, the cooling distance exceeds the magnetic field correlation length, which we assumed to be $l_c \sim 1$ Mpc. This changes the energy dependence in Eq. (4) because the energy-dependent cooling distance must be replaced by the constant correlation length. Furthermore, integration over energies in the cascade affects the power-law behavior. For these reasons, our basic estimates in section 2 were not expected to capture all the features evident in the numerical results.

The proton delay is strongly dependent on the high energy cutoff of the cosmic ray source, which affects the energy at which the proton delays begin to dominate. This can be seen in Fig. 9. This behavior is further illustrated in Fig. 4 and Fig. 6, where one can see that the proton delays begin to dominate at $E \sim 10$ TeV for a proton high energy cutoff of 10^8 GeV and an IGMF $= 10^{-15}$ G.

The distribution of gamma-ray arrival times depends on the injection spectrum of protons, as one can see from a comparison of Fig. 4 and Fig. 5. This is in contrast with the *spectra* of gamma rays, which are *not* sensitive to the proton injection spectrum (Essey et al. 2010, 2011a). Hence, one can, at least in principle, learn about the proton injection spectrum from timing observations, but not from the spectra alone. (Neutrino spectra also depend on the proton injection spectrum (Essey et al. 2010).) Furthermore, stochastic broadening illustrated in Fig. 7 also affects the predictions.

Based on our results, the observed time variability should be washed out on time scales shorter than ~ 0.1 yr, for distant blazars ($z > 0.2$), at TeV and higher energies. Time variability can be present for $z > 0.2, E > 1$ TeV on the time scales of $0.1 - 1$ yr. If gamma rays with $E \sim 10^2$ TeV are observed, they can exhibit variability on shorter time scales.

Of course, one must also consider the delays the cosmic rays undergo at the source. Blazars are known to be highly variable, and this variability could affect the shape of the observed spectrum. The magnetic fields within galaxies are on the order of 1 μG which can lead to significant delays in the source. On the other hand, the structure of magnetic fields in front of the blazar jets is not known. Furthermore, the effect of the source variability

would be to suppress the observed power of the source by a factor

$$f_{\rm damp} \sim N_{\rm active} \left(\frac{t_{\rm active}}{t_{\rm delay}} \right), \tag{28}$$

where $t_{\rm delay}$ is the typical proton delay at the source, $t_{\rm active}$ is the typical time the source is active or flaring and $N_{\rm active}$ is the number of times the source is active in the time period $t_{\rm delay}$. This damping should not be a significant effect (Dermer et al. 2011), especially since the typical deflections at the source are not big enough to affect the beaming factors assumed in popular models.

An alternative situation is that the magnetic fields within the blazar jet are not randomly distributed, but are, instead, strongly correlated with the direction of the jet. Blazar jets emit an extremely large amount of charged matter and the wind in the direction of the jet can eliminate any random-field configuration that one usually expects in a galaxy. Thus, it is possible that cosmic rays escape the source along the jet with very small time delays, preserving the intrinsic variability of the source. In this case, delays in the intergalactic medium can broaden the intrinsic variability to the energy dependent timescales of these delays.

At energies where the optical depth of the observed gamma rays is below one, we expect the signal to be primary gamma rays, and any variability in this signal is indicative of the source variability. This variability should not depend strongly on the energies of the gamma rays, but rather on the scale of the structure at the source producing the gamma rays.

However, we expect a very different behavior for energies at which primary gamma rays are significantly attenuated by pair production off EBL. In the case of strongly correlated magnetic fields in the jet, we expect that the variability should show different structure in the low energy component, where it should depend on the energy. The spectrum should show variability on shorter timescales for higher energies until some critical energy $E_c \sim$ TeV, where the timescales cease to decrease further, thanks to the domination of the cosmic ray contribution. In the case of large delays within the source, we expect all variability to be washed out at these higher energies (typically around a TeV for most observed sources).

Some exceptionally bright flares can come through around E_c and rise above the *pedestal* created by the stochastic arrival times of protons. Such flares should have distinctly softer spectra than the hard pedestal, which can be a means of distinguishing these flares from the stochastic pedestal.

For most of discussion, we have assumed that IGMFs have strengths are of the order of a femtogauss. This range is suggested by the spectral fits to the data Essey et al. (2011b). However, field strengths well below a femtogauss can be consistent with the data as well.

In the case of very weak IGMFs, the time delays become smaller, since $\tau \propto B^2$. For $B \sim 10^{-18}$ G, the time delays can be as short as minutes.

We have also assumed that the strength of IGMF is constant on average, which is a good assumption for propagation in the voids. However, if the line of sight intersects a filament of stronger, *e.g.*, nanogauss magnetic field, the reduction of the secondary photon signal depends on the size of the filament and on its location. Thin filaments can only intercept as small fraction of protons within the 0.1 degree associated with a given source. However, a thick filament or a sheet of strong field can deflect protons, reducing the secondary signal.

Temporal structure of gamma-ray signals can be used to measure the IGMF structure and EBL intensity in different directions, on a source-by-source basis. In addition, it may provide a way to probe the high energy cutoff of cosmic ray sources, as well as the spectrum of EBL. A statistical analysis on multiple bins of data is needed to determine the variability at different energies. This presents challenges at the highest energies because of the low statistics, but longer observation times and the advent of next generation experiments should make this analysis increasingly powerful.

6. Acknowledgments

The authors thank S. Ando and K. Murase for helpful discussions. The work of W.E. and A.K. was supported in part by DOE grant DE-FG03-91ER40662. A.K. appreciates the hospitality of the Aspen Center for Physics, which is supported by the NSF grant No. PHY-1066293.

REFERENCES

HESS Collaboration, Abramowski, A., et al. 2010, A&A, 520, A83

Aharonian, F., Essey, W., Kusenko, A., & Prosekin, A. 2012, arXiv:1206.6715

Aharonian, F. A., Timokhin, A. N., & Plyasheshnikov, A. V. 2002, A&A, 384, 834

Kelner, S. R., & Aharonian, F. A. 2008, Phys. Rev. D, 78, 034013

Aharonian, F. A., Kelner, S. R., & Prosekin, A. Y. 2010, Phys. Rev. D, 82, 043002

Aharonian, F. A., Khangulyan, D., & Costamante, L. 2008, MNRAS, 387, 1206

Alcock, C., & Hatchett, S. 1978, ApJ, 222, 456

Berezinsky, V., Gazizov, A., & Grigorieva, S. 2006, Phys. Rev. D, 74, 043005

de Angelis, A., Roncadelli, M., & Mansutti, O. 2007, Phys. Rev. D, 76, 121301

Dermer, C. D., Cavadini, M., Razzaque, S., Finke, J. D., & Lott, B. 2011, ApJ, 733, L21

Essey, W., & Kusenko, A. 2010, Astropart. Phys., 33, 81

Essey, W., Kalashev, O. E., Kusenko, A., & Beacom, J. F. 2010, Phys. Rev. Lett., 104, 141102

Essey, W., Kalashev, O., Kusenko, A., & Beacom, J. F. 2011a, Astrophys. J., 731, 51

Essey, W., Ando, S., & Kusenko, A. 2011b, Astropart. Phys., 35, 135

Essey, W., & Kusenko, A. 2011, ArXiv e-prints, arXiv:1111.0815

Horns, D., & Meyer, M. 2012, J. Cosmology Astropart. Phys., 2, 33

Ichiki, K., Inoue, S., & Takahashi, K. 2008, ApJ, 682, 127

Katarzyński, K., Ghisellini, G., Tavecchio, F., Gracia, J., & Maraschi, L. 2006, MNRAS, 368, L52

Lefa, E., Rieger, F. M., & Aharonian, F. 2011, ApJ, 740, 64

Murase, K., Takahashi, K., Inoue, S., Ichiki, K., & Nagataki, S. 2008, ApJ, 686, L67

Murase, K., Dermer, C. D., Takami, H., & Migliori, G. 2011, ArXiv e-prints, arXiv:1107.5576

Mücke, A., Engel, R., Rachen, J. P., Protheroe, R. J., & Stanev, T. 2000, Computer Physics Communications, 124, 290

Protheroe, R. J., & Meyer, H. 2000, Physics Letters B, 493, 1

Razzaque, S., Dermer, C. D., & Finke, J. D. 2012, ApJ, 745, 196

Stecker, F. W., & Scully, S. T. 2007, A&A, 478, L1

Szabo, A. P., & Protheroe, R. J. 1994, Astroparticle Physics, 2, 375

Taylor, A. M., Ahlers, M., & Aharonian, F. A. 2011, Phys. Rev. D, 84, 105007

Williamson, I. P. 1972, MNRAS, 157, 55

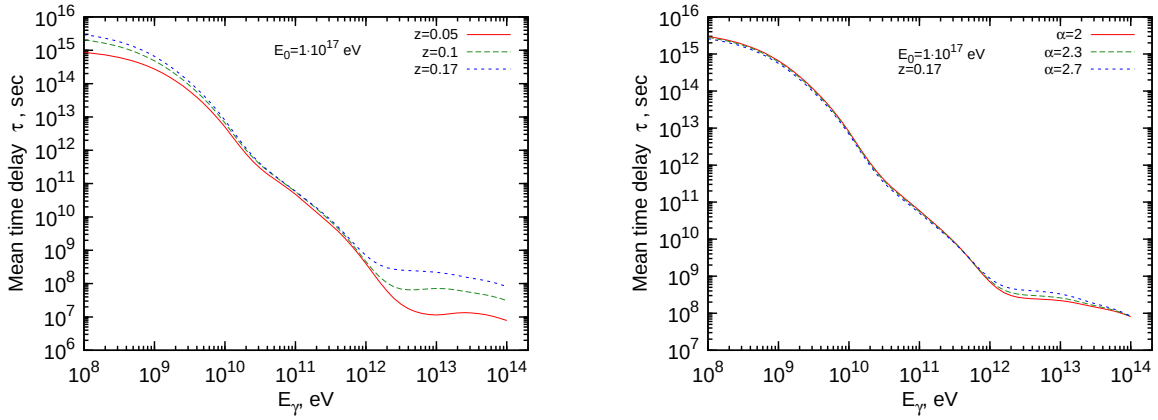

Fig. 3.— Left panel: mean time delay of gamma rays for the sources at different redshifts and the proton spectrum with cutoff energy $E_0 = 10^{17}$ eV. Right panel: mean time delay of gamma rays for the source at $z = 0.17$ and the proton spectrum with cutoff energy $E_0 = 10^{17}$ eV and different spectral indices α.

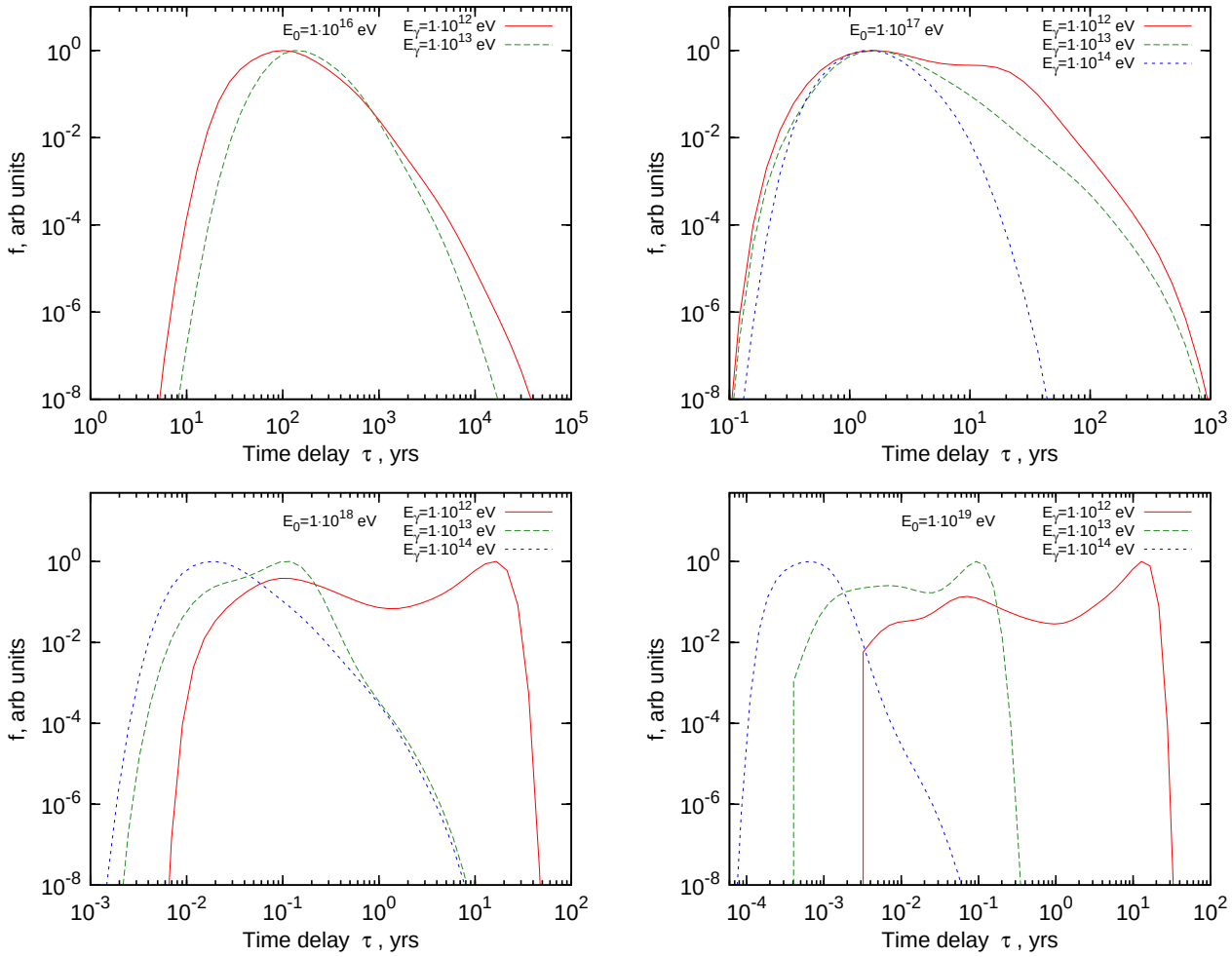

Fig. 4.— Time delay distribution of gamma rays in arbitrary units (the maximum of distribution is normalized to unity) at different energies from the source at $z = 0.17$. Each plot corresponds to the proton spectrum with different cutoff energy E_0 and spectral index $\alpha = 2$. The injected spectra of protons are taken in the range from $0.1E_0$ to E_0.

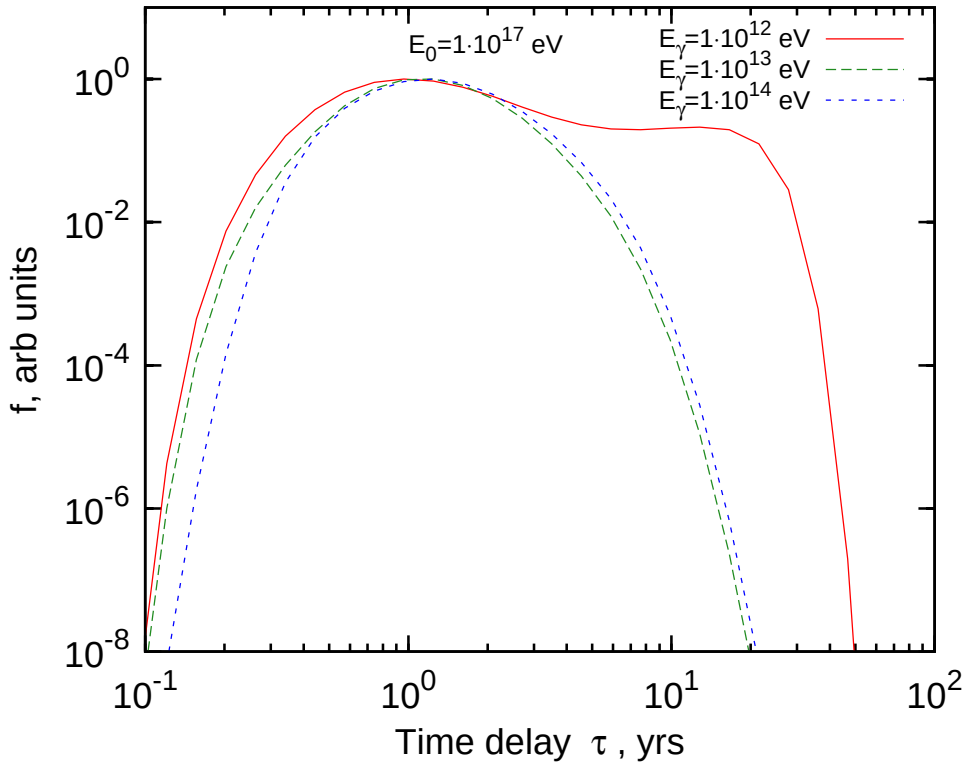

Fig. 5.— Time delay distribution of gamma-ray in arbitrary units (the maximum of distribution is normalized to unity) from the source at $z = 0.17$. The injected spectrum of protons is almost monoenergetic with energy $E = 10^{17}$ eV.

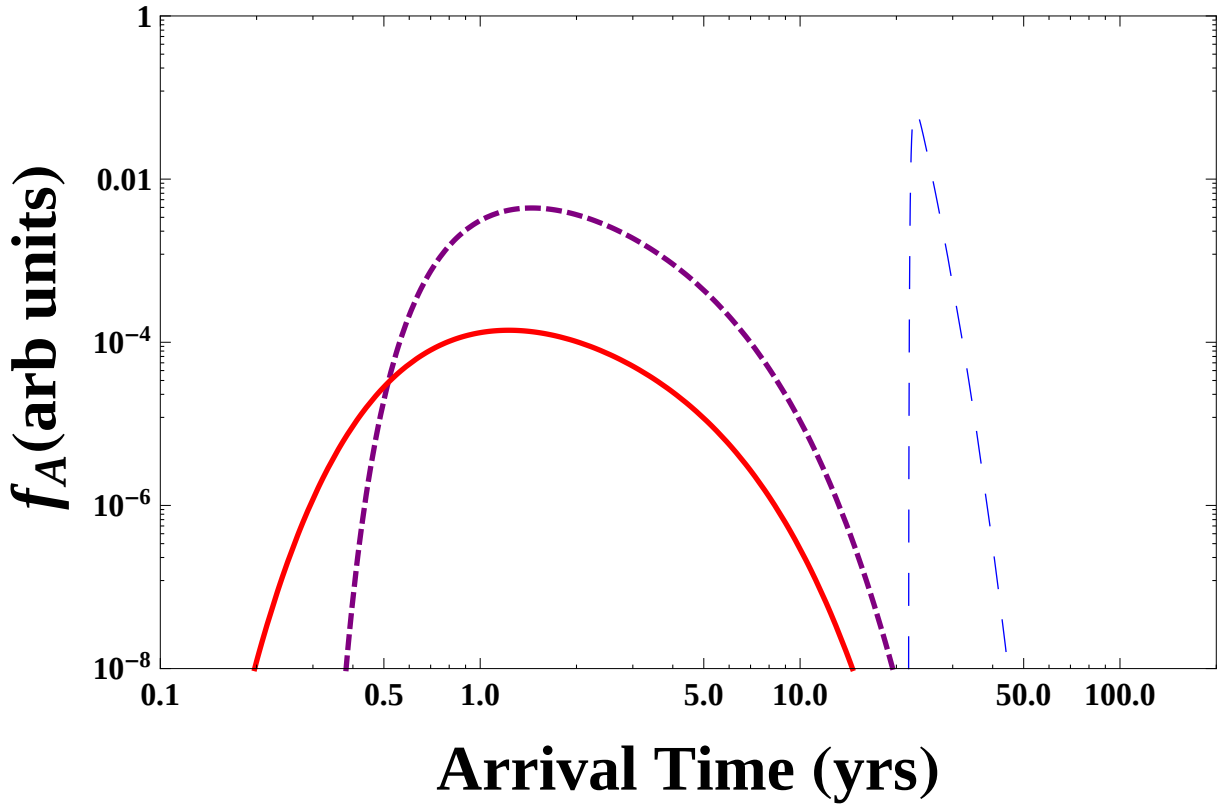

Fig. 6.— Arrival time probability distribution in arbitrary units for secondary gamma rays with energies 1 TeV (blue, long-dashed line), 10 TeV (purple, short-dashed line) and 100 TeV (red, solid line). Results are shown for a cosmic ray source at $z = 0.2$ with a high energy cutoff of 10^8 GeV and an IGMF of 10^{-15} G.

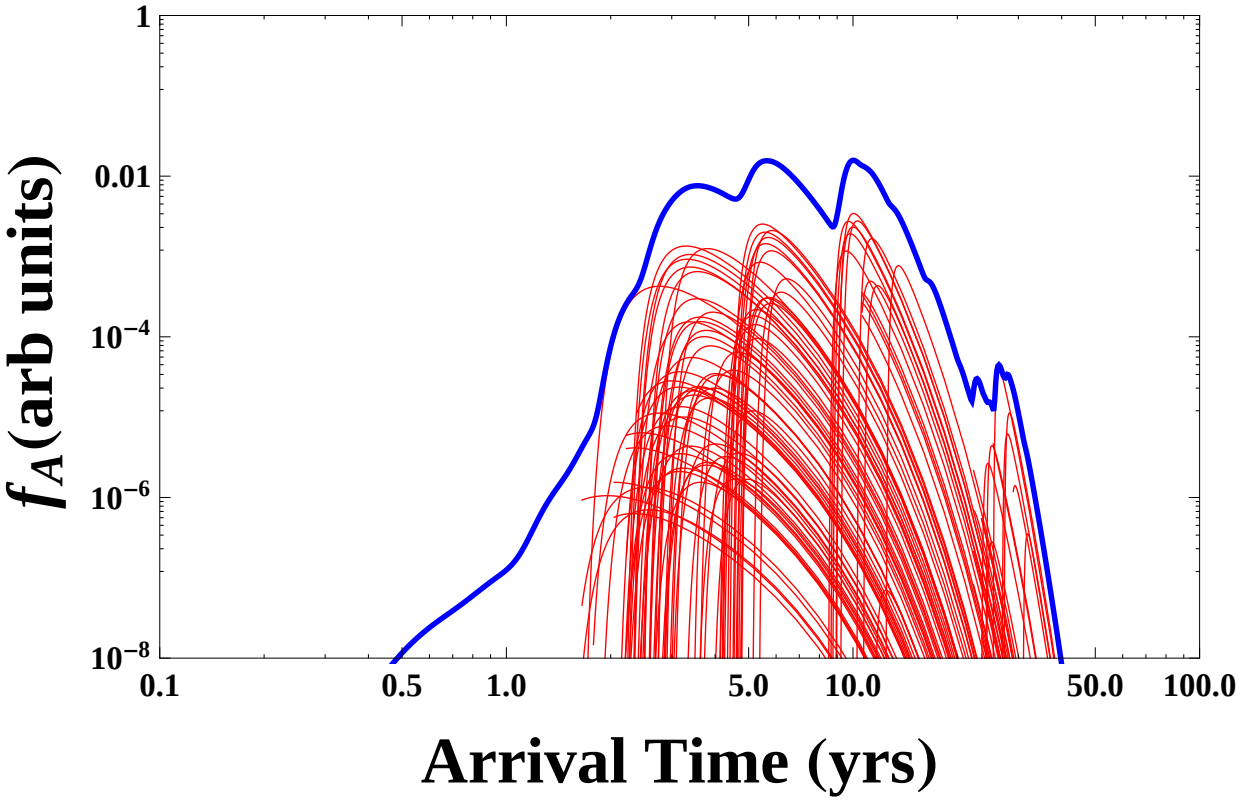

Fig. 7.— Arrival time probability distribution in arbitrary units for 1 TeV secondary photons for multiple numerical runs. The results shown are for roughly 300,000 secondary photons with an IGMF of 10^{-15} G and UHECR cutoff of 10^{10} GeV. The blue thick line represents the sum of all distributions and the thin red lines are a representative set of distributions.

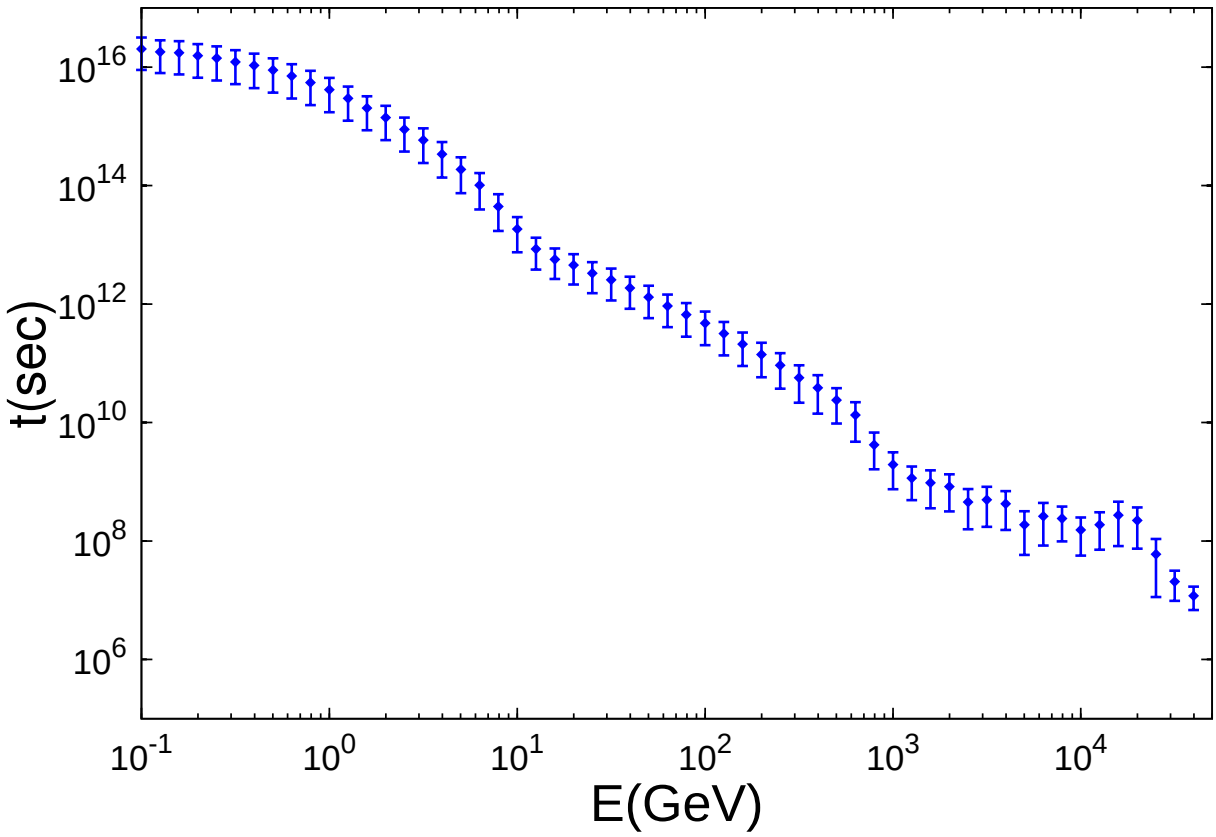

Fig. 8.— Arrival time delays from an instantaneous pulse emitted by a source at $z = 0.2$, assuming $B = 10^{-15}$ G with $l_c = 1$ Mpc correlation length.

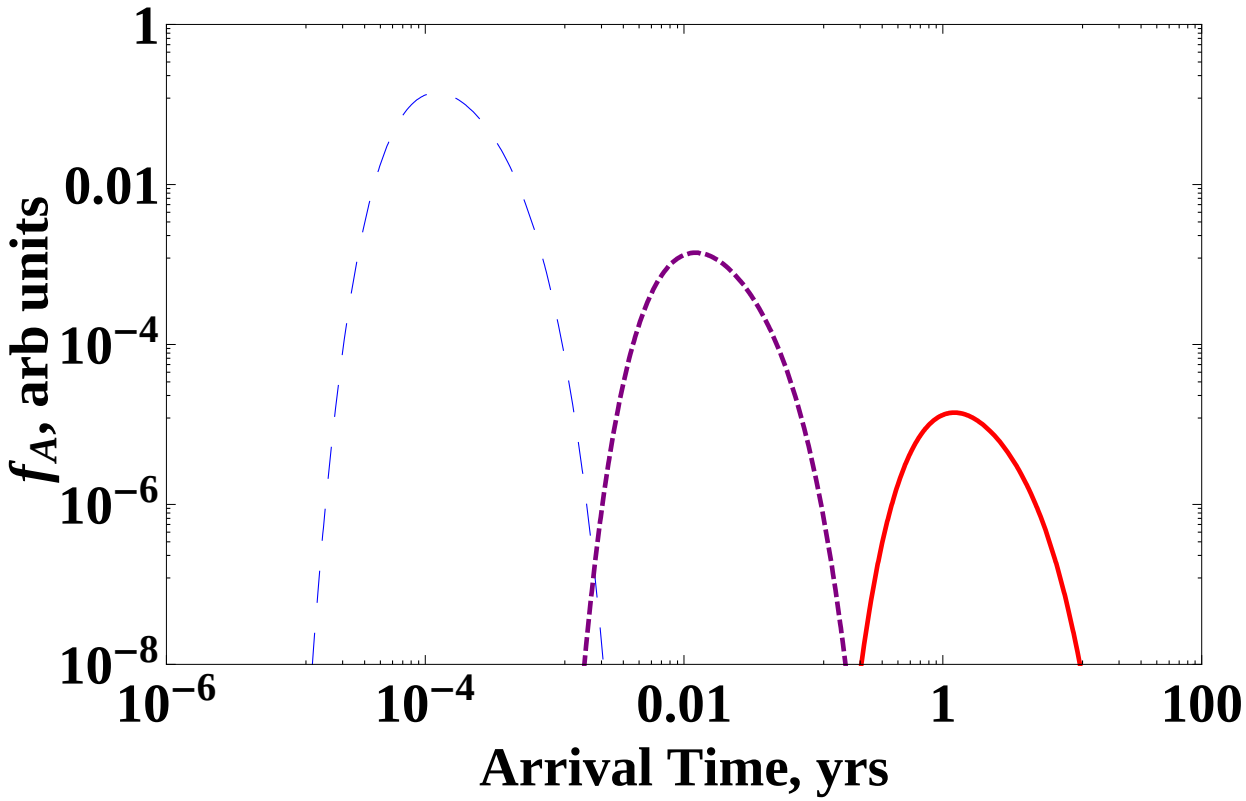

Fig. 9.— Arrival time probability distribution in arbitrary units for primary cosmic rays. Results are shown for a cosmic ray source at $z = 0.2$ with a high energy cutoff of 10^{10} GeV (blue, long dashed), 10^{9} GeV (purple, short dashed) and 10^{8} GeV (red, solid) and an IGMF of 10^{-15} G.